nature biomedical engineering

Supplementary information

https://doi.org/10.1038/s41551-025-01501-w

# Minimally invasive implantation of scalable high-density cortical microelectrode arrays for multimodal neural decoding and stimulation

In the format provided by the authors and unedited

**Supplementary Information**

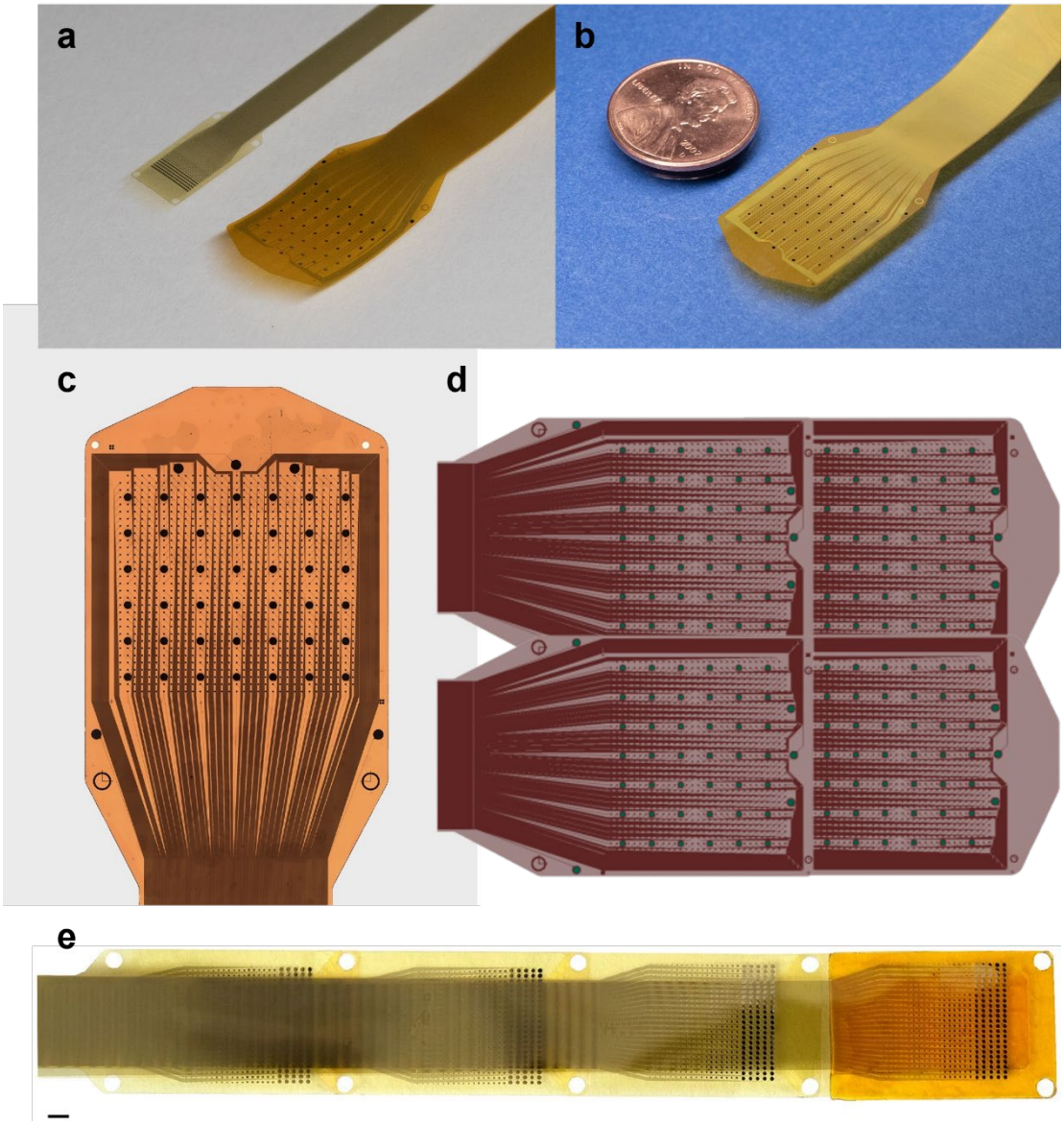


**Supplementary Figure 1: Individual and modular configurations of 1024-channel and 529-channel thin-film micro-electrocorticography arrays provide configurable options for cortical surface interfaces.** (a) Device photographs of 529-channel (left) and 1024-channel (right) thin-film microelectrode arrays. (b) Photograph of 1024-channel thin-film microelectrode array with penny for scale. (c) Device photograph of two modularly connected 1024-channel thin-film microelectrode arrays. (d) Computer-aided design showing one possible modular (2-by-2) configuration of four 1024-channel arrays for simultaneous implantation of 4096 microelectrodes over 6.24 $cm^2$ of cortical surface area. (e) Modular configurations of multiple 529-channel arrays can also be constructed. Shown here is a quadruply-connected assembly of four 529-electrode modules with a single pocket, for simultaneous implantation of 2116 microelectrodes over 1.92 $cm^2$ of cortical surface area. Scale bar: 1 mm.

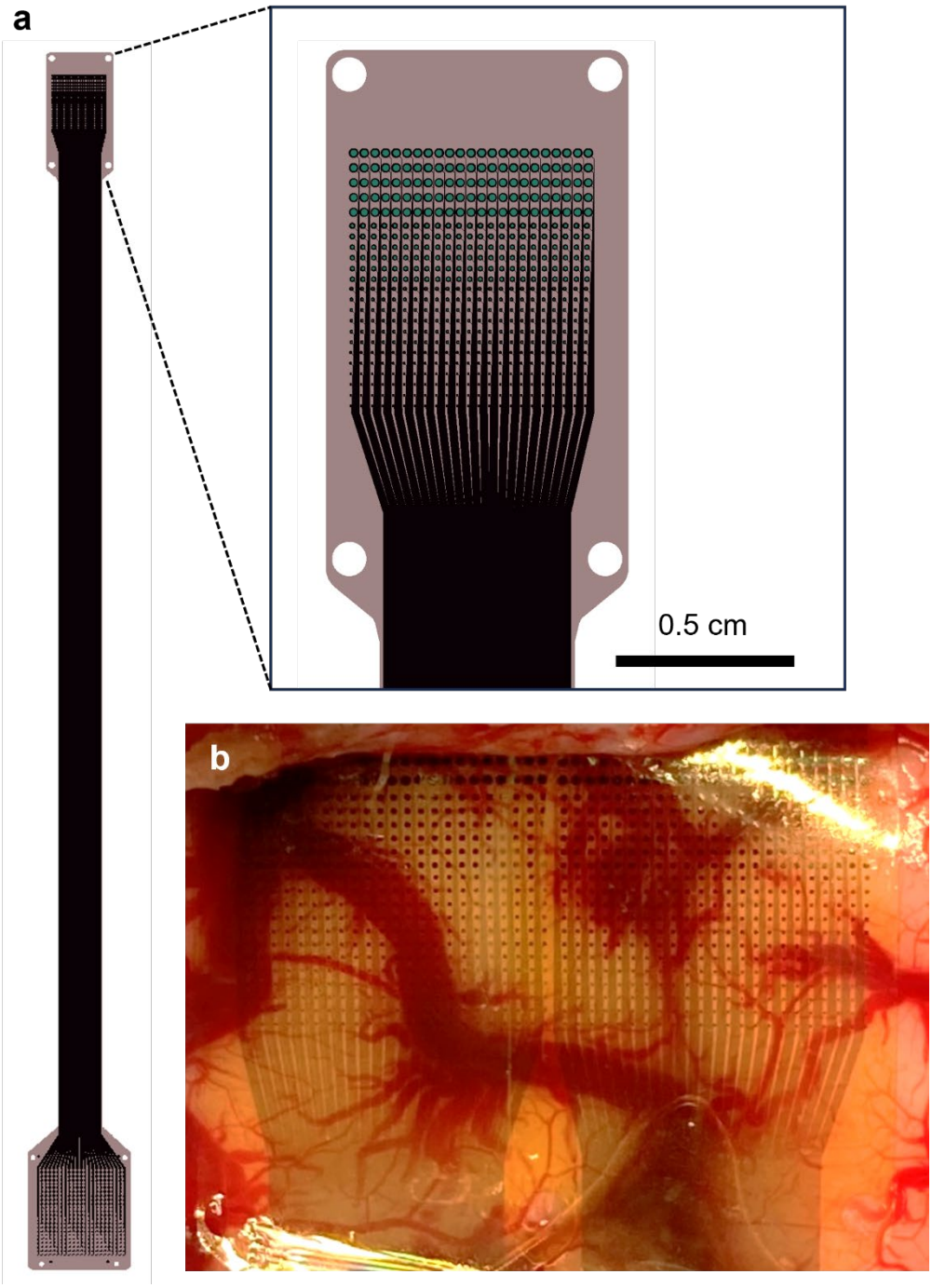


**Supplementary Figure 2: Detailed renderings and device images of 529-channel thin-film micro-electrocorticography arrays.** (a) Computer-aided design showing the entire 529-channel device, including electrode array, traces, and connector region. The inset shows the electrode array in greater detail. (b) Device photograph of two modularly connected 529-channel thin-film microelectrode arrays *in situ* on the exposed cortical surface during microelectrocorticographic recording via craniotomy in a Göttingen minipig.

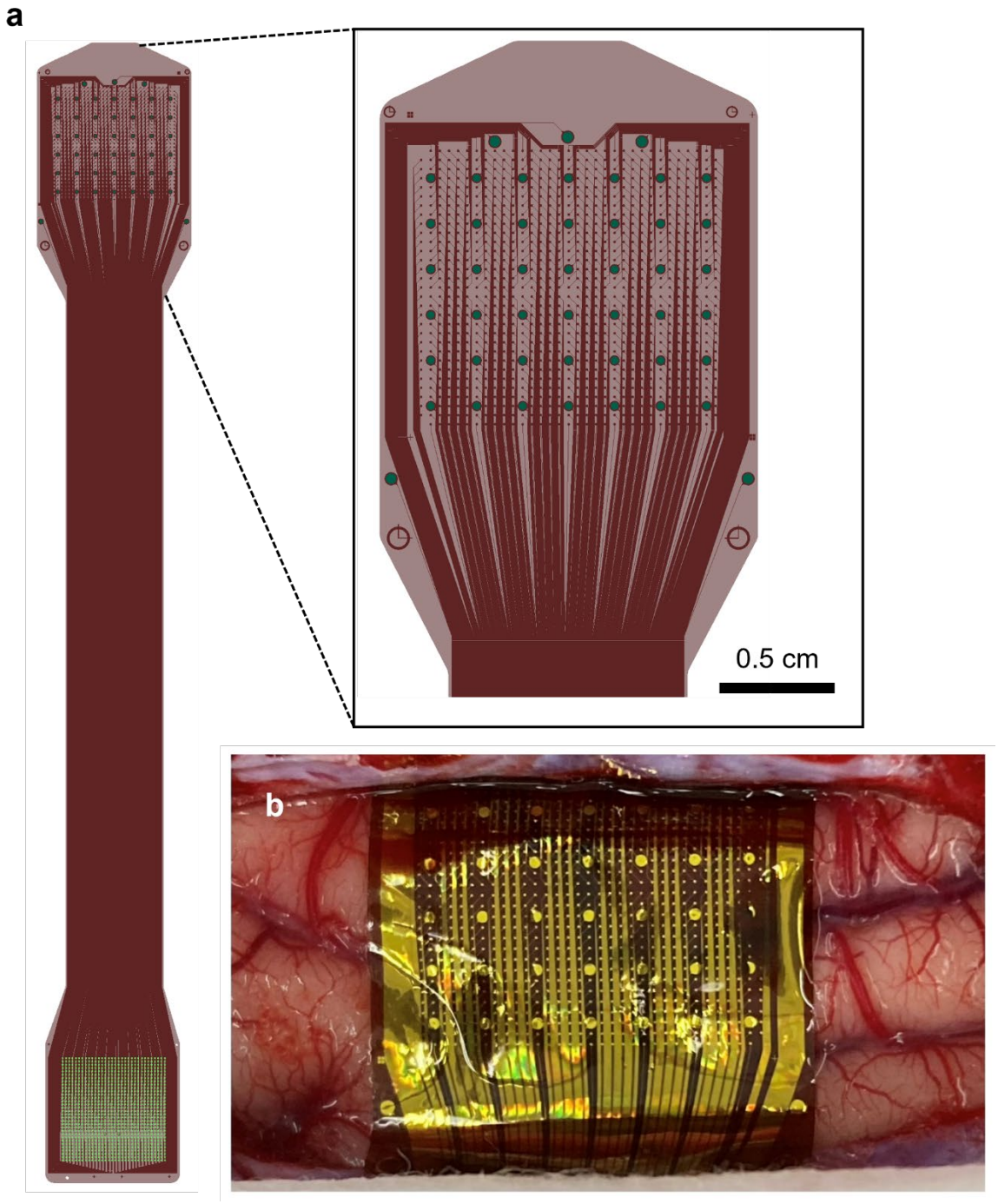


**Supplementary Figure 3: Detailed renderings and device images of the 1024-channel thin-film micro-electrocorticography array.** (a) Computer-aided design showing the entire 1024-channel device, including electrode array, traces, and connector region. The inset shows the electrode array in greater detail. (b) Device photograph of 1024-channel thin-film microelectrode arrays *in situ* on the exposed cortical surface during microelectrocorticographic recording via craniotomy in a Göttingen minipig.

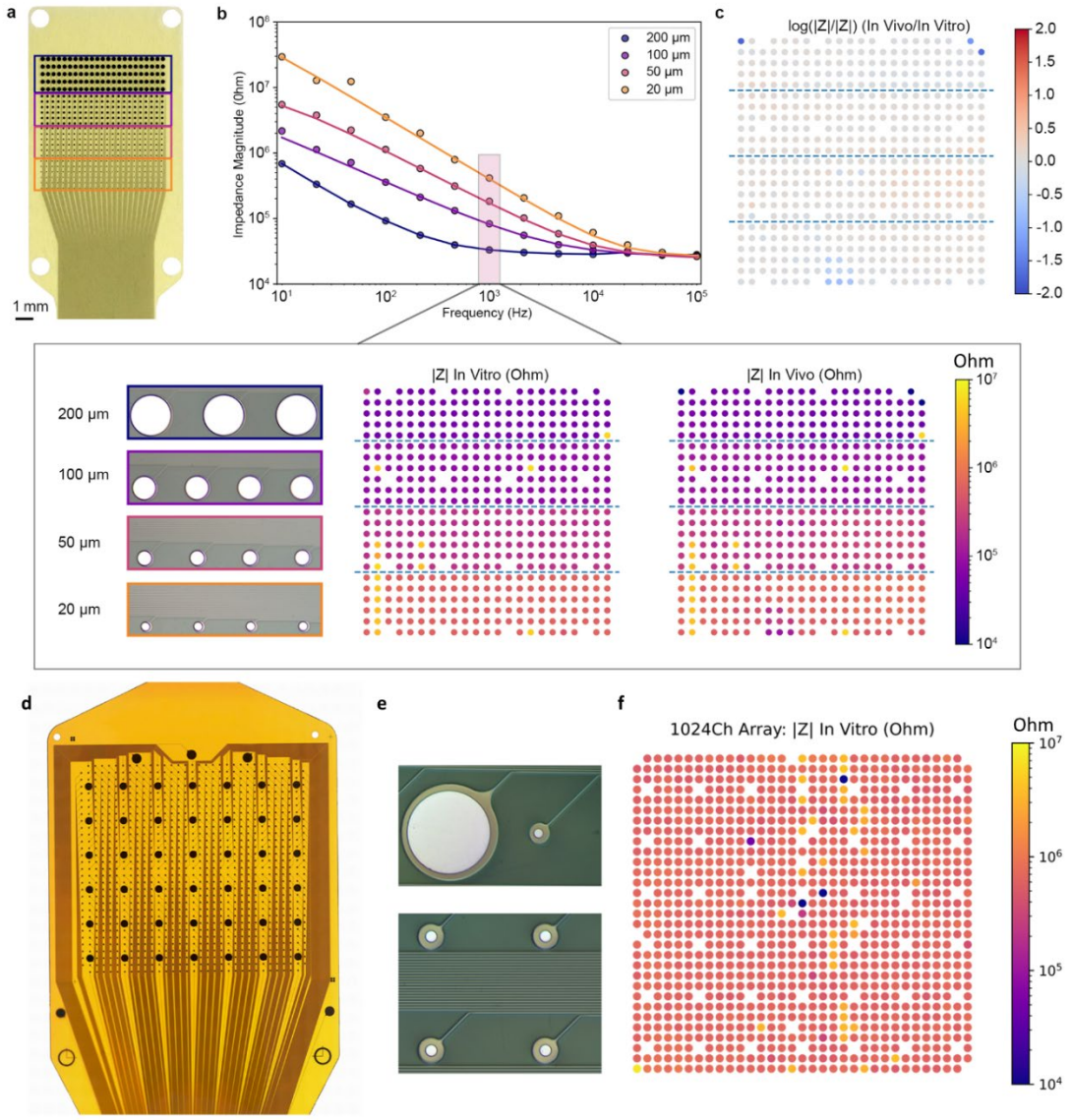


**Supplementary Figure 4. Electrode characterization.** (a) Photograph of a single array with 200, 100, 50, and 20 µm electrodes outlined by blue, purple, pink, and orange boxes, respectively. (b) *In vitro* electrochemical impedance spectroscopy (EIS) spectra for each electrode size, with equivalent circuit fits based on a Randles circuit. (Inset) *In vitro* (left) and *in vivo* (right) impedance maps of recording channels over a complete 529-channel array, measured at 1 kHz, with microscope images for each electrode size included as references. Stimulation and ground channels are shown as gaps in the plots. (c) Map of the ratio between *in vivo* and *in vitro* impedance at 1 kHz, displaying minimal change across most of the array following implantation. (d) Photograph of a 1024-channel array configuration, with reference electrodes around the periphery and stimulation (large) and recording (small) electrodes, respectively, in the main rectangular cluster. (e) Micrographs showing detailed views of 380-micron stimulation (top) and 50-micron recording electrodes (bottom), with nearby trace routing also depicted. (f) Impedance map of recording electrodes only, measured at 1 kHz. (Stimulation electrodes are routed and measured separately from the record electrodes, as external pads, not pictured.)

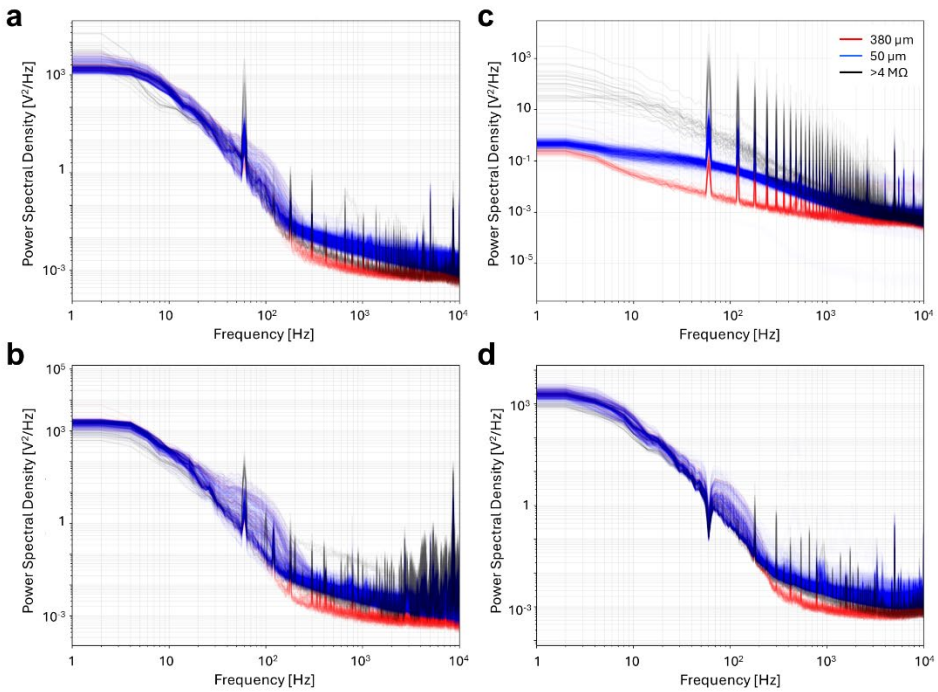


**Supplementary Figure 5. Power spectra.** The power spectral densities obtained under various conditions *in vivo* and *in vitro*: (a, b) Free-running electrocorticography in two different anesthetized Göttingen minipigs, (c) Free-running recording *in vitro*, (d) Free-running electrocorticography in an anesthetized Göttingen minipig with a 60-Hz notch filer applied. Distributions were calculated using Welch's method from 30-second recording epochs split into 0.5 second segments, with 0.25 second overlap; the Hann window was used. Distributions are shown for each of the principal electrode types (50 µm and 380 µm), as well as for rejected electrodes (impedance greater than 4 MΩ).

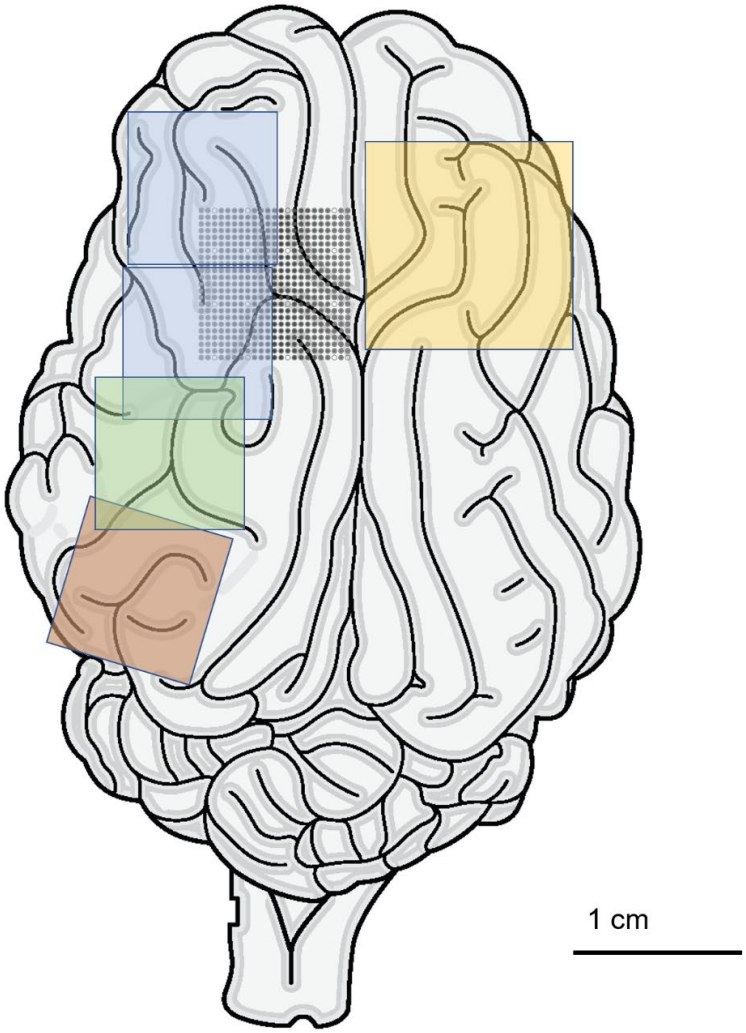


**Supplementary Figure 6. Cortical regions accessed in the Göttingen minipig using surface microelectrode arrays.** Multiple functional regions of the Göttingen minipig brain were accessed in 26 animals during the course of these investigations. Array locations are shown here in schematic fashion. Although many experiments involved bilateral array placement, for clarity of illustration 529-channel array silhouettes are shown here over the left hemisphere, and a 1024-channel array is shown over the right hemisphere. Yellow, 1024-channel array over rostrum somatosensory and limb, face, and mouth motor regions. Blue, 529-channel arrays over rostrum somatosensory regions; green, 529-channel array over auditory cortex; brown, 529-channel array over visual cortex. Black dots, 529-channel array over limb, face, and mouth motor regions, each dot representing a single recording electrode.

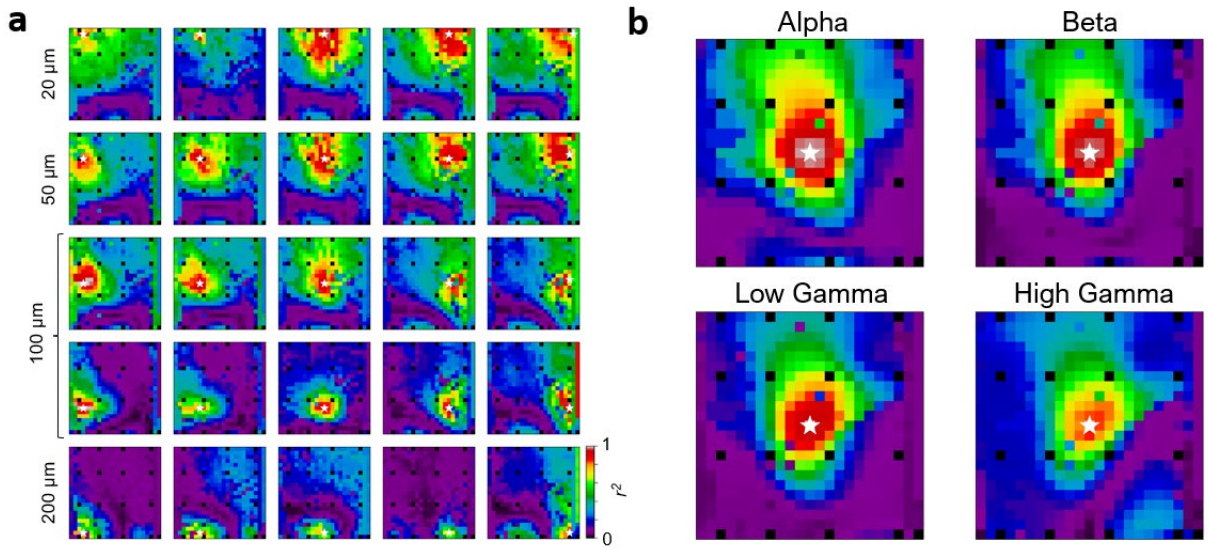


**Supplementary Figure 7. Spatial scales of information representation on the cortical surface.** The degree to which closely spaced microelectrodes across a single 529-channel array record correlated or uncorrelated information is relevant to neural decoding and is illustrated graphically in these heatmaps. The data shown here were recorded on a single 529 channel electrode array. Black pixels correspond to electrodes wired for stimulation and not available for use in the correlation analysis. (a) Correlation map of the Pearson correlation coefficient $r^2$ computed for unfiltered signals recorded during spontaneous cortical activity, with correlations across the entire array in each sub-plot referenced to one of 25 representative electrodes (white stars) distributed evenly over the array. Each row contains electrodes of the same contact diameter, which is indicated by the labels on the left hand side of each row. Correlations are computed over 2-second windows averaged over 50 trials. (b) Correlation map for different EEG bands recorded on a single representative electrode, illustrating larger regions of relatively stronger correlation (red and orange) at lower frequencies. Alpha band is defined as 8-12 Hz, beta band as 12-30 Hz, low-gamma band is defined as 30-55 Hz, and high gamma band is defined as 65-120 Hz.

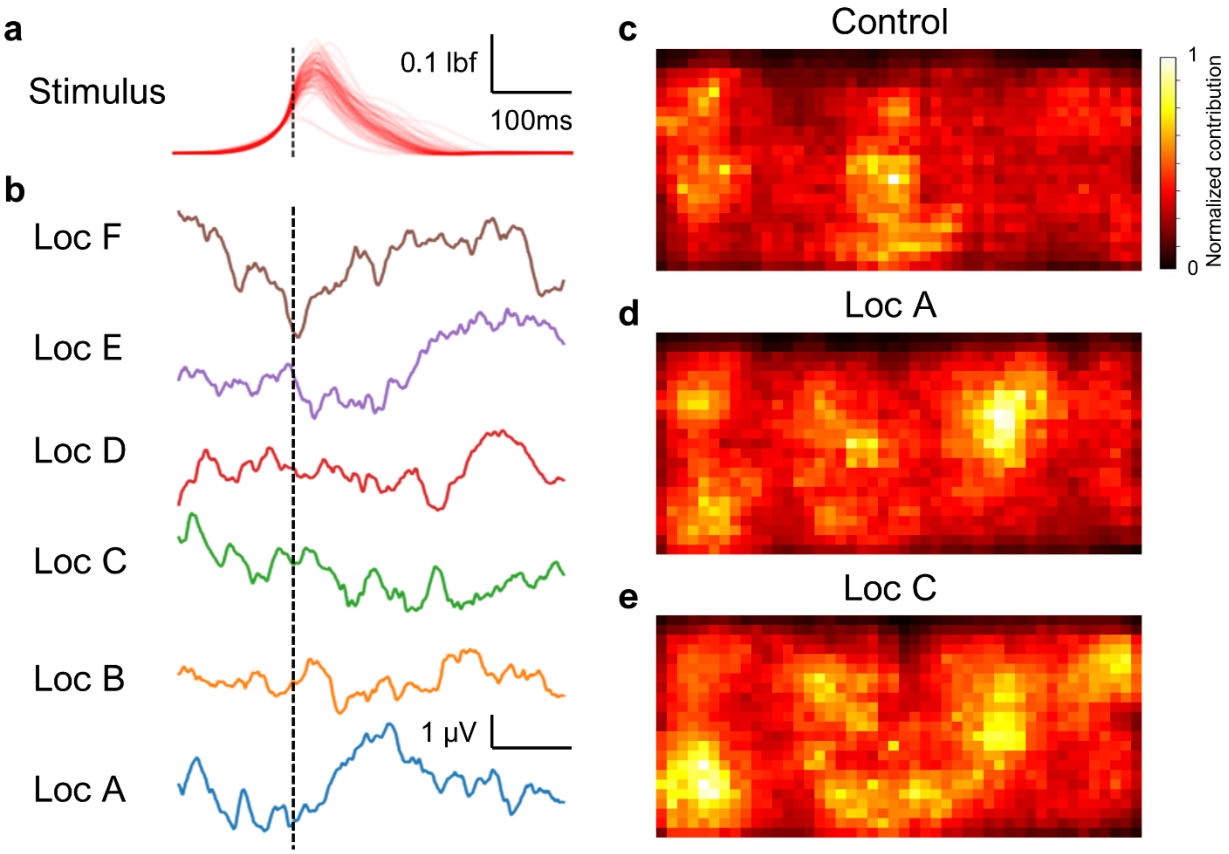


**Supplementary Figure 8. Saliency maps.** (a) Force profile of 100 tactile stimuli (1 red line per trial) applied to the rostrum. All trials were time aligned to reaching 0.1 lbf of the rising edge. (b) Rostrum somatosensory evoked potential (SSEP) averaged over 130 trials for each stimulation location as shown in Figure 4a. The right column shows examples of average saliency maps for decoding single-shot (c) spontaneous trials (control), (d) stimulation at location A and (e) location C. The color scale is normalized to the maximum value for each stimulation location independently.

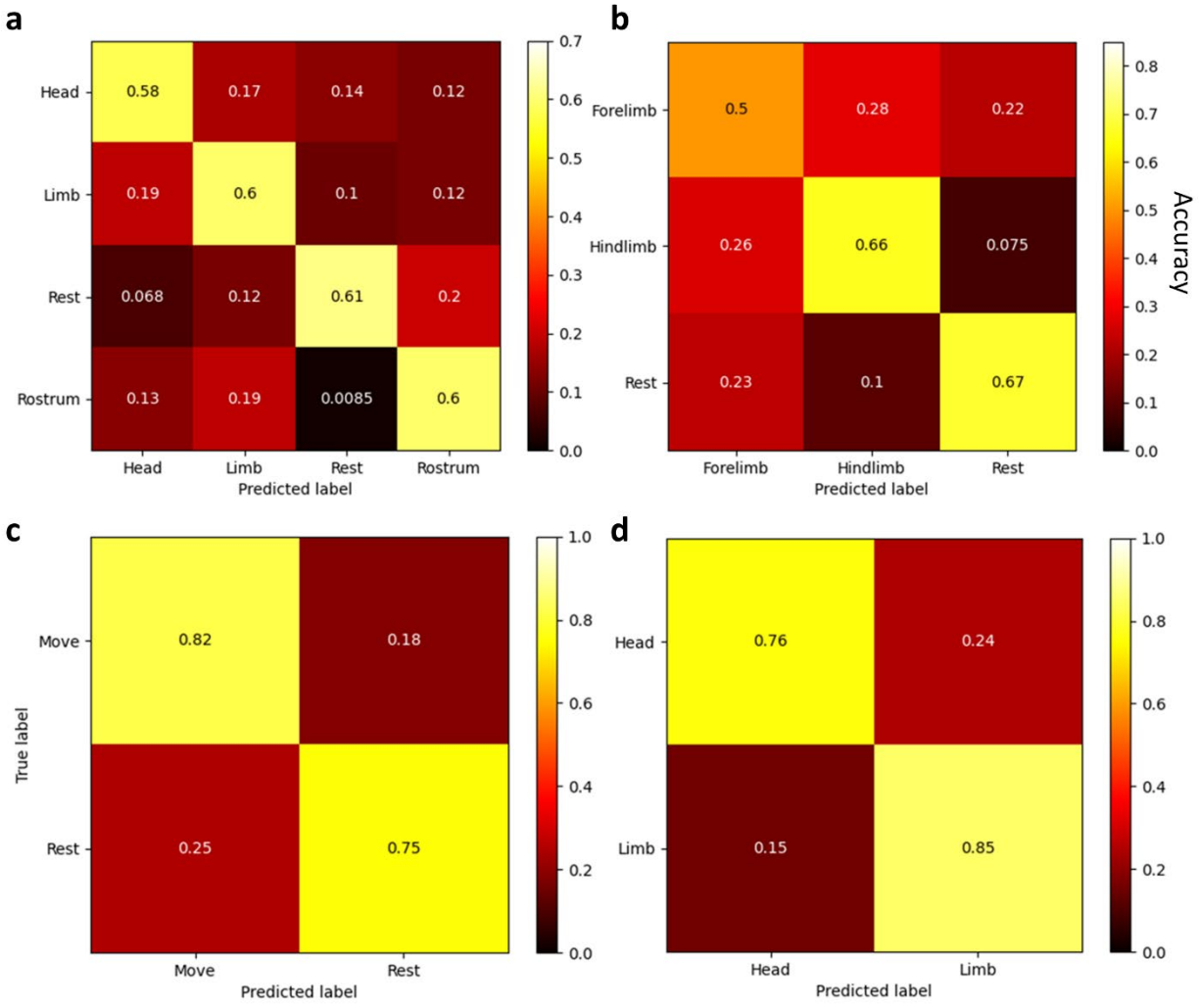


**Supplementary Figure 9. Versatile motor decoding paradigms from sensorimotor region.** Confusion matrices from decoding sensory and motor modalities of various body regions (*k*-fold cross-validation; *k*=5). (a) Classification of head movement, limb movement, rest, and sensory stimulation of the rostrum (Accuracy: 60%). (b) Classification of forelimb movement, hindlimb movement, and rest (Accuracy: 61%). (c, d) Classification of general movement versus rest (Accuracy: 79%) and head versus limb movements (Accuracy: 80%).

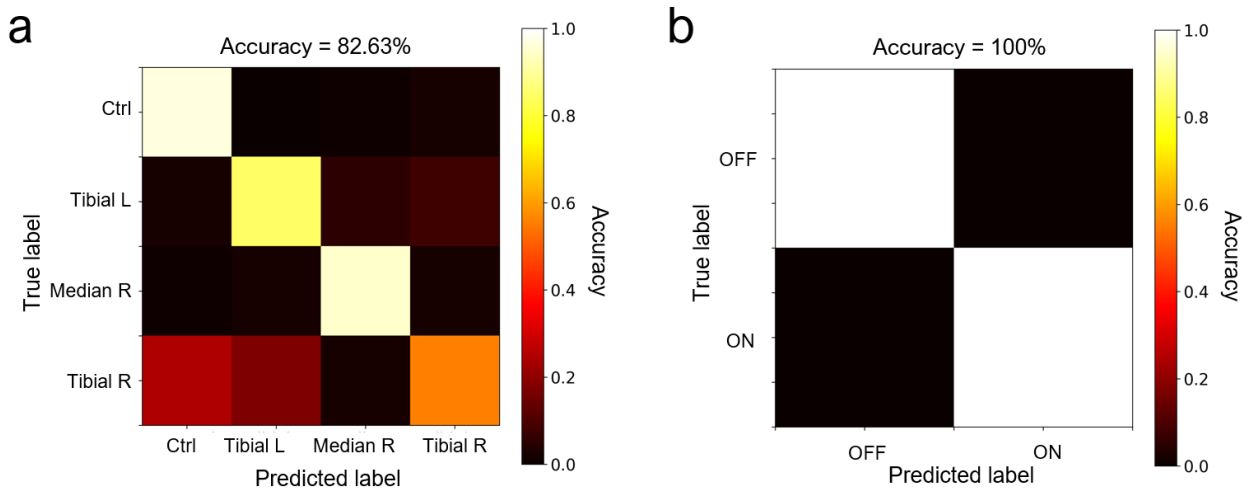


**Supplementary Figure 10. Multimodal neural decoding of somatosensory and visual information.** (a) Confusion matrix for decoding somatosensory evoked potentials (SSEPs) induced through electrical stimulation of the median and tibial nerves (*R*, right; *L*, left. (b) Confusion matrix for decoding light flashes from the visual cortex as presented to the contralateral eye.

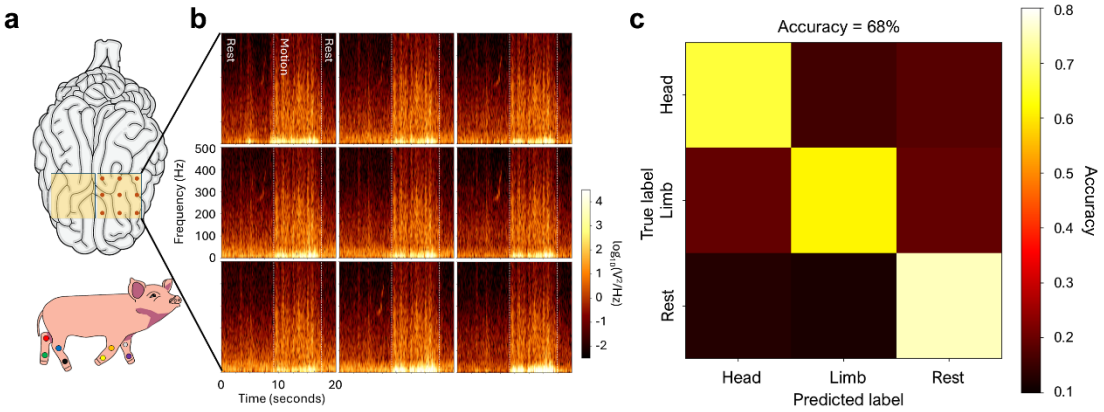


**Supplementary Figure 11. Awake motor decoding.** (a) Schematic showing bilateral placement of 1024-channel electrode arrays (2048 microelectrodes total) for motor decoding during volitional walking (inset schematic). (b) Illustrative subsamples of spectrograms drawn from the group of electrodes indicated as red dots in (a) across the array, corresponding to each of two forelimb movement states, stationary (0-9 s) and moving (10-18 s), demonstrating grossly distinct, state-dependent patterns of cortical activity. (c) Decoding of limb movements from pre-movement microelectrocortical activity. Confusion matrix of decoding limb movement and rest state using pre-movement neural activity with a convolutional neural network (CNN), with 10-fold cross-validation (the training set comprised 127 separately observed gross motor events of each type, and the test set comprised a balanced dataset of 32 events).

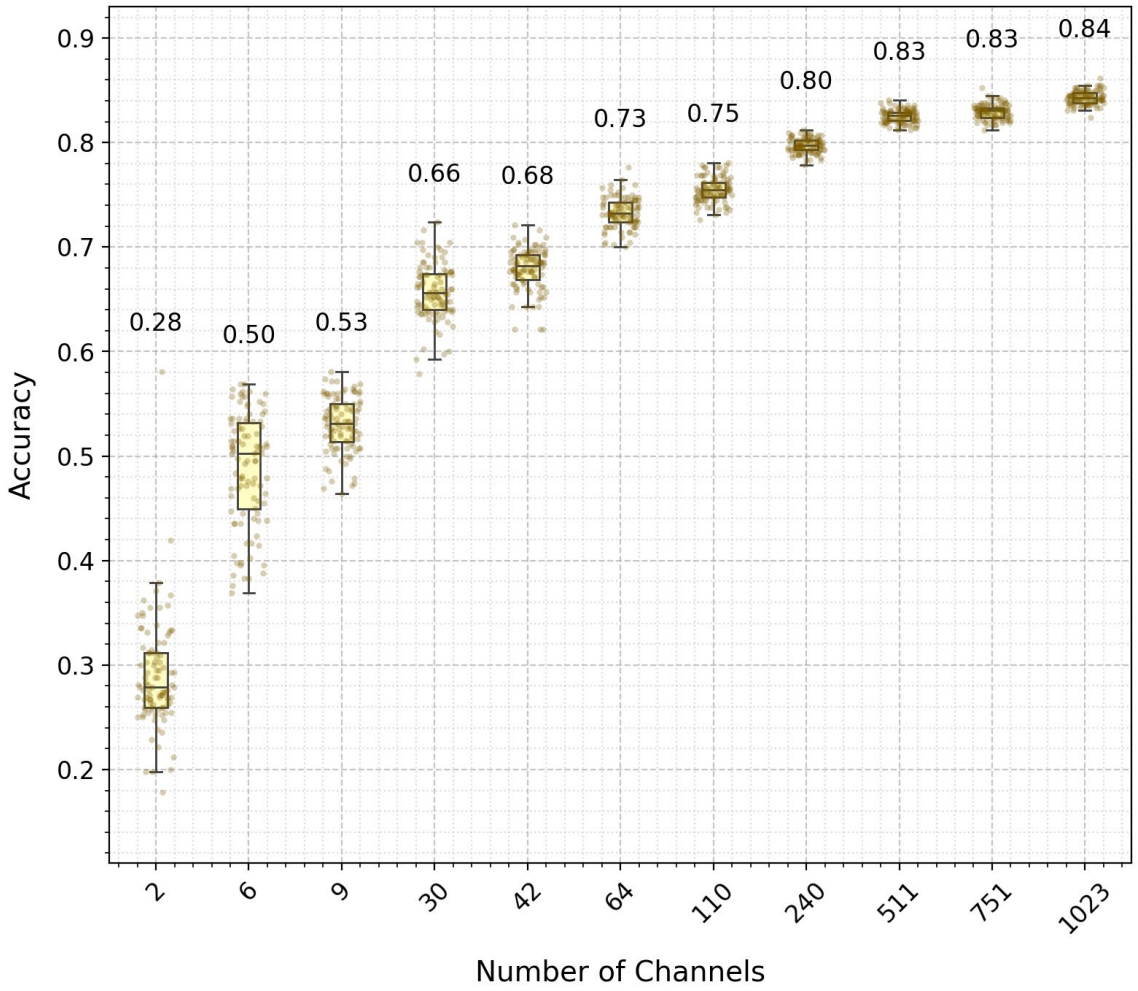


**Supplementary Figure 12. Improving neural decoding performance as a function of microelectrode number and spatial density.** For the neural decoding problem of 14-class somatosensory discrimination as described in the main body of the manuscript, the dependence of decoding performance on electrode number and spatial density was assessed. For each of 11 sub-grids of various sizes ("Number of Channels") subsampled from the full complement of 1024 electrodes (yet spanning the full surface area of the array), 100 models (light brown dots) were independently trained.and tested. The results are shown as a whisker plot, illustrating monotonically improving neural decoding performance and decreasing variance in performance with increased electrode number and spatial density. The highest mean performance is 84% (chance corresponds to 7%), reached using the full complement of 1024 electrodes, though performance does not appear to have reached an asymptote at this level.

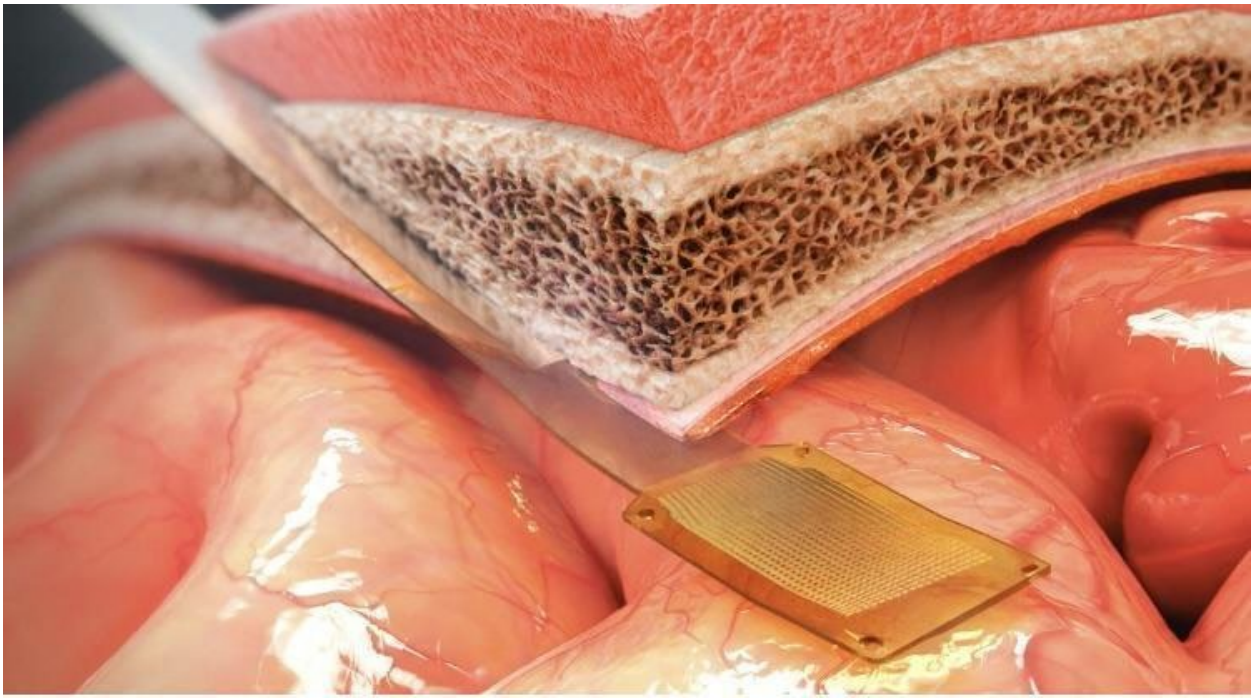

**Supplementary Video 1: Cranial microslit insertion technique for placement of thin-film microelectrode arrays.** This video demonstrates the cranial microslit insertion technique. The first segment illustrates forming the microslit at an approach angle tangent to the cortical surface target using a sagittal saw, first in the setting of an intact skull, then in a cut-away view. The next segment demonstrates the technique being employed *in vivo* in a Göttingen minipig. The final segment demonstrates the cranial microslit technique being used to perform subdural insertion of a 1024-channel microelectrode array in a human cadaver. (Link to Supplementary Video 1.)

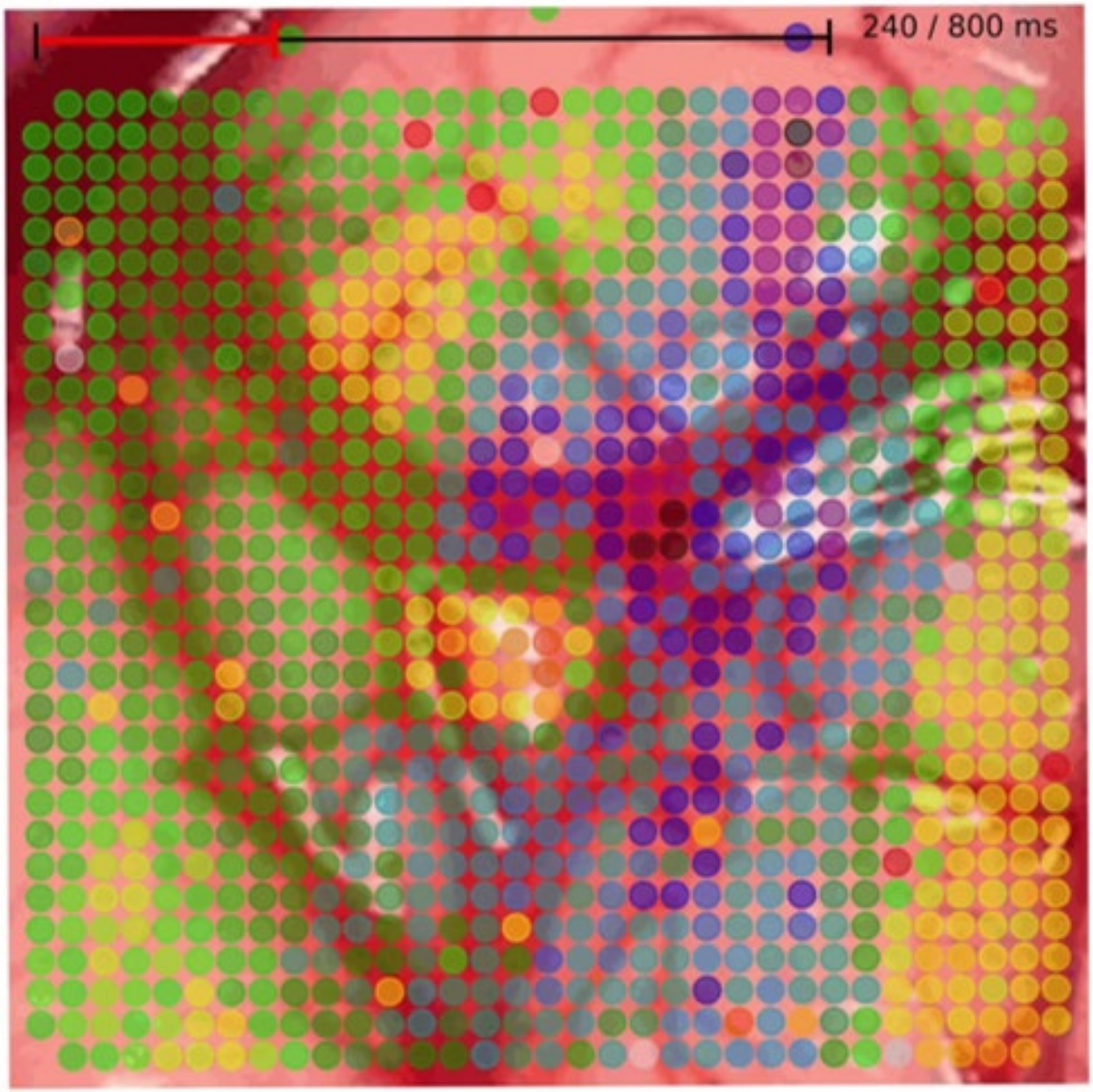


**Supplementary Video 2: Thin-film microelectrode arrays provide high-resolution neural recordings from the cortical surface in real time under anesthesia.** After implantation of a 1024-channel microelectrode array in a Göttingen minipig, neural recordings were obtained in the absence of any external stimulation, representing spontaneous electrocortical activity, as described in the manuscript. The video shows full-bandwidth neural recordings from one 1024-channel electrode array (right hemisphere) as a color-map of voltage, superimposed on and aligned to an image of the underlying cortical surface (each dot corresponds to one microelectrode in the array). (Link to Supplementary Video 2.)

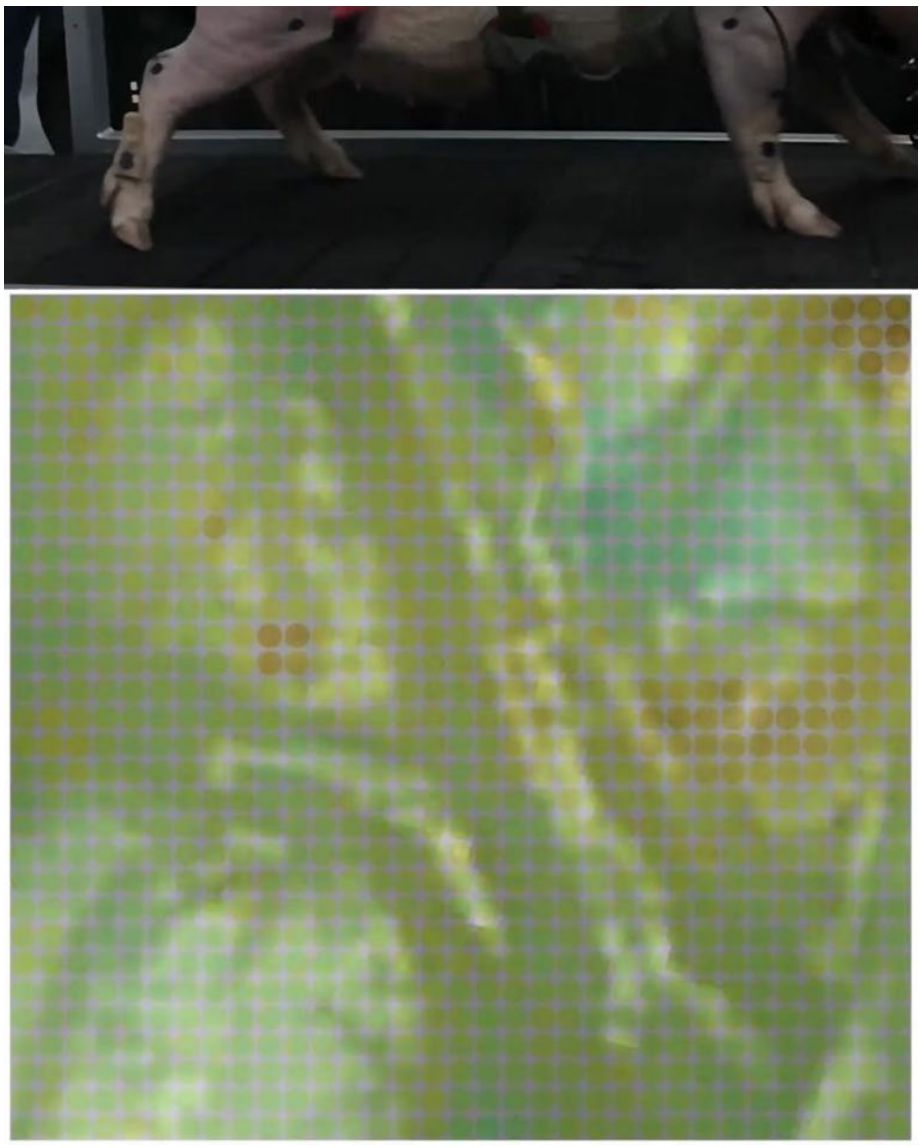

**Supplementary Video 3: Thin-film microelectrode arrays provide high-resolution neural recordings from the cortical surface in real time during volitional walking.** After bilateral implantation of two 1024-channel microelectrode arrays (one per hemisphere over sensorimotor cortex in a Göttingen minipig), the animal was awakened and permitted to walk ad lib on a treadmill. Head- and limb-based accelerometers and real-time motion tracking image capture data were time-synchronized with full-bandwidth neural recordings, and these data were used for neural decoding of volitional limb movement, as described in the manuscript. The video shows full-bandwidth neural recordings from one 1024-channel electrode array (left hemisphere) as a color-map of voltage, superimposed on and aligned to an image of the underlying cortical surface (each dot corresponds to one microelectrode in the array); limb movement during treadmill walking is shown in the top panel, time-aligned to the displayed neural recording. (Link to Supplemental Video 3.)

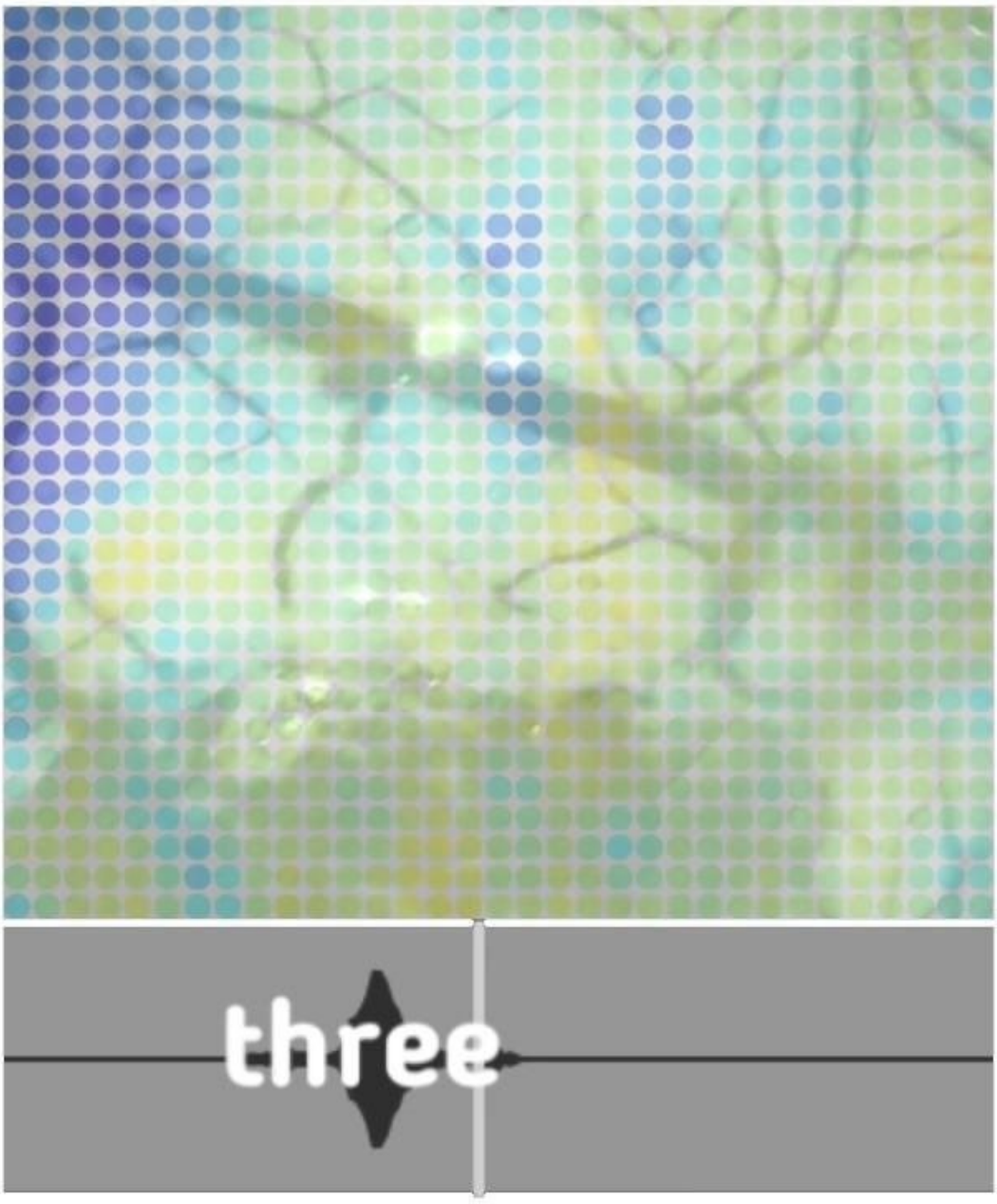


**Supplementary Video 4: High-resolution neural recordings from the cortical surface during speech.** Thin-film microelectrode arrays provide high-resolution neural recordings in real time during awake language mapping in a human neurosurgical patient. The video demonstrates the final phase of conventional cortical mapping (monopolar stimulation) followed by placement of the 1024-channel thim-film microelectrode array. Following array placement, the video shows a digital overlay-representation of electrocortical activity superimposed on an image of the cortical surface. Each colored disc represents a microelectrode placed in the corresponding location. The time-evolving color map represents normalized raw voltage as obtained from the digital steps of the analog-to-digital converter (*dark blue*, low; *yellow*, high). The time-synchronized audio amplitude of the cued words being spoken is shown in the lower panel, with superimposed textual annotation of the spoken words. (Link to Supplementary Video 4.)